

# Formation and Evolution of Ultraluminous X-ray Pulsar Binaries to Pulsar-Neutron Star and Pulsar-White Dwarf Systems

K. Abdusalam<sup>1</sup>, Iminhaji Ablimit<sup>2,3,\*</sup>, P. Hashim<sup>4</sup>, G.-L Lü<sup>5,1</sup>, M. K. Mardini<sup>6,2</sup>, and Z.-J Wang<sup>1</sup>

## ABSTRACT

Recent observational and theoretical results have suggested that some of ultraluminous X-ray (ULX) sources may contain neutron star (NS) accretors. However, the formation channel and properties of donor stars of NS ULXs remain uncertain. By adopting the non-conservative and rotation-dependent mass transfer model in the primordial binary evolution, we investigate the way to form pulsar ULXs like observed pulsar ULXs in a systematic way. Our simulation results indicate that pulsar ULXs with Be stars and intermediate or/and high mass donors match observed apparent luminosities, orbital periods and observationally indicated donor masses of known pulsar ULXs. ULXs with Be and intermediate donors are main contributors. The route of accretion-induced collapse of WDs has 4.5% contribution to the NS ULXs, 4.0% of NSs in ULXs are formed through electron-capture supernovae (SNe), and 91.5% of NSs in ULXs are born with core-collapse SNe. We also studied the evolution of pulsar ULXs to double compact star systems. We do not find NS-black hole systems (merging in a Hubble time) that evolved from pulsar ULXs. Pulsar-white dwarf (WD) cases that evolve through pulsar ULXs have significant contributions to the whole NS-WD gravitational wave sources. Contributions of pulsar-WD and pulsar-NS

---

<sup>1</sup>School of Physical Science and Technology, Xinjiang University, Urumqi 830046, China

<sup>2</sup>Key Laboratory for Optical Astronomy, National Astronomical Observatories, Chinese Academy of Sciences, Beijing 100012, China; iminhaji@nao.cas.cn

<sup>3</sup>Department of Astronomy, Kyoto University, Kitashirakawa-Oiwake-cho, Sakyo-ku, Kyoto 606-8502, Japan; iminhaji@kustastro.kyoto-u.ac.jp

<sup>4</sup>Astronomical Observatory of Xinjiang, Chinese Academy of Sciences, Urumqi 830046, China

<sup>5</sup>Center for Theoretical Physics, Xinjiang University, Urumqi 830046, China; guolianglv@xao.ac.cn

<sup>6</sup>Shandong Provincial Key Laboratory of Optical Astronomy and Solar-Terrestrial Environment, Institute of Space Sciences, Shandong University, Weihai 264209, China

★ Corresponding Author

cases that experienced pulsar ULXs are  $\sim 40\%$  and  $11\%$  among all LISA NS-WD and NS-NS sources, respectively. Monte Carlo simulation noise with different models give a non-negligible uncertainty.

*Subject headings:* Binary stars (154); X-ray binary stars (1811); Stellar evolution (1599); Neutron stars (1108); Gravitational waves (678); Pulsars (1306); White dwarf stars (1799)

## 1. Introduction

The Ultra-luminous X-ray sources (ULXs) were first discovered in nearby galaxies (e.g., Fabbiano 1989), and ULXs are point-like off-nuclear extragalactic sources with an X-ray luminosity of  $L_X \geq 10^{39} \text{ erg s}^{-1}$  (see the review Kaaret et al. 2017). The super- or sub-Eddington accretion onto stellar-mass black holes (BHs) or intermediate mass BHs has been suggested as the power sources of the high X-ray luminosity of ULXs (e.g. Colbert & Mushotzky 1999; Feng & Soria 2011). Recently, pulsations in the X-ray data of nine ULXs have been observed (see Table 1), and the apparent X-ray luminosities in those ULXs are higher than the Eddington limit for a typical neutron star (NS), and the observed pulsations in these ULXs provided irrefutable evidence that those ULXs contain accreting NSs (Bachetti et al. 2014; Fürst et al. 2016; Tsygankov et al. 2017; Israel et al. 2017; Carpano et al. 2018; Brightman et al. 2018; Sathyaprakash et al. 2019).

The emission mechanism (producing high apparent luminosity) and formation channel of ULXs are two main debates addressed in the last decades. For the first argument, the presence of geometrically thick accretion disks was invoked to produce the observed high luminosities of ULXs by causing beaming emission (Shakura & Sunyaev 1973; King et al. 2001; King 2009; Poutanen et al. 2007). The very strong magnetic field ( $B \sim 10^{14} \text{ G}$ ) of the magnetar-like NS was proposed as one possible physical mechanism to increase the effective luminosity by reducing the electron scattering cross-section (e.g., Herold 1979; Dall’Osso, Perna & Stella 2015; Mushtukov et al. 2015). However, King & Lasota (2019) suggested that the observed ULX properties are explained by NSs with normal magnetic fields and not by the presence of magnetars, and Table 1 of King & Lasota (2020) shows derived magnetic field strengths of pulsar ULXs are lower than that of a normal magnetar. Besides, the highly super-Eddington accretion disc that extends close to the accretor without the very strong magnetic field was studied to generate the extreme luminosities (e.g. Kluźniak & Lasota 2015). For the observed correlation between pulse fraction and X-ray photon energy in pulsar ULXs, King & Lasota (2020) suggested that NS spin axes significantly misaligned from their central accretion discs, and discussed that scattering in the funnels collimating

their emission and producing their apparent super-Eddington luminosities is the most likely origin of the correlation. To explore the exact emission process to produce super-Eddington luminosities, more observational evidences and investigations are required.

In the second argument, the nature of donor stars is the most uncertain property of ULXs. Observationally, the far distances, bright accretion disks, and the significant variations in the spectra of ULXs from year to year make the donor stars and their properties hard to detect (see Kaaret et al. (2017) and Heida et al. (2019) for more discussions). There are rough mass estimations for seven pulsar ULXs (see Table 1), and observational results indicate that high mass or intermediate mass stars are more likely be donors in ULXs. In the theoretical frameworks for the formation channel, Fragos et al. (2015) investigated the origin of the NS ULXs. They considered non-conservative mass transfer and specific orbital angular momentum loss due to the mass loss in the population synthesis simulation code BSE (Hurley et al. 2002) and detailed binary calculation of the MESA code (Paxton et al. 2015). Initial masses of  $3 - 8 M_{\odot}$  in relatively short orbital periods (1-3 days) have been suggested for NS ULXs by Fragos et al. (2015). Subsequently, the binary population synthesis (BPS) study of Wiktorowicz et al. (2017) demonstrated that NS X-ray binaries may significantly contribute to the ULX population compared to BH X-ray binaries (see also Shao & Li (2015)), and showed that donor stars in NS ULXs tend to have lower masses ( $< 2 M_{\odot}$ ). BPS results of Wiktorowicz et al. (2019) found that most BH ULXs have isotropic X-ray emissions, while beaming X-rays are more common in NS ULXs. Misra et al. (2020) modeled detailed evolution of low- and intermediate-mass ( $\sim 0.92 - 8 M_{\odot}$ ) X-ray binaries by using the MESA code and considering beaming effects, tides, general angular momentum losses, and a detailed/self-consistent calculation of the mass transfer rate. They discovered that some observational properties of pulsating ULXs can be reproduced by intermediate mass X-ray binaries if non-conservative mass transfer and geometrical beaming are adopted. They also studied detectable NS-white dwarf (WD) systems that evolved from ULXs with intermediate-mass donors. Before this, Marchant et al. (2017) and Finke & Razzaque (2017) explored that ULXs can be progenitors of compact objects as the gravitational wave (GW) sources.

In this work, we studied formation and evolution of ULX pulsar binaries by considering a wide range of physical information in the binary evolution. We presented evolutions of binary systems to pulsar ULXs with Be stars, helium stars and low, intermediate and massive stars (including non-Be main-sequence and (sub)giant-branch stars). We also investigated the final outcomes of ULXs and their contribution to the compact objects (NS-NS and NS-WD systems) as the gravitational sources. In §2, we describe our method to treat the binary physical processes in the simulation. The calculated properties and birth rates are given in §3. The ULX contributions of NS-NS and NS-WD systems to LISA detection are also

discussed in §3. The discussion and conclusion are in §4.

## 2. Binary Evolution Model and Calculations

### 2.1. Simulation of Binaries

We simulate the binary evolutionary processes which start from a primordial system of two zero-age main-sequence (ZAMS) stars, and main processes include mass transfer, stellar winds, tidal interaction, angular momentum evolution, supernova explosions and natal kicks, common envelope (CE) evolution, magnetic braking, GW radiation, merger, etc.

We run a large number ( $3 \times 10^7$ ) of binary evolution calculations by applying the updated *BSE* population synthesis code based on Hurley et al. (2000, 2002). For the SN remnant calculation, we adopted the rapid remnant-mass model of Fryer et al.(2012) in the subroutine *hrdiag* of the updated code, and note that a typo in Fryer et al. (2012) has been corrected in our code (corrected as  $a_1 = 0.25 - \frac{1.275}{(M_1 - M_{\text{proto}})}$ , also in the calculations of Ablimit & Maeda (2018)). In the subroutine *evol2* of this updated *BSE* code, we employ a mass transfer model related to the rotation of the accretor (Ablimit et al. 2016), because Ablimit & Maeda (2018) found that profiles of formed compact objects with this model are consistent with observed properties of the gravitational sources. Instead of using empirical results for the critical mass ratio of Hurley et al. (2002), the numerically calculated one based on the rotation-dependent mass transfer model by considering both the response of the secondary to mass accretion and the effect of possible mass loss (see Ablimit et al. (2016)) is used. In this non-conservative and rotation-dependent mass transfer model, the rotation of the secondary star (the star with a lower mass is defined as the secondary) affects its accretion rate by a factor of  $(1 - \omega/\omega_{\text{cr}})$ , where  $\omega$  is the angular velocity of the secondary star and  $\omega_{\text{cr}}$  is its critical value (Petrovic et al. 2005; de Mink et al. 2009). The secondary star can spin faster to close its its critical value if the star accretes a small amount of mass (Packet 1981), and this makes the mass transfer efficiency as low as  $< 0.2$ . Thus, the maximal initial mass ratio of the primary to the secondary stars in primordial binaries for avoiding the contact phase can reach  $\sim 5$ -6, and a larger number of the primordial binaries can experience stable mass transfer phases until the primary’s envelope is completely exhausted (e.g., de Mink et al. 2013). If the mass transfer is unstable (the primary is a evolved star), the binaries are assumed to be a contact ones and enter a CE phase. The two stars can merge into a single star with the other case.

For the CE evolution of a binary, the standard energy conservation equation (Webbink

1984) is adopted in the subroutine *comenv* of the code,

$$E_{\text{bind}} = \alpha_{\text{CE}} \Delta E_{\text{orb}} , \quad (1)$$

where  $E_{\text{bind}}$ ,  $\alpha_{\text{CE}}$ , and  $\Delta E_{\text{orb}}$  are the binding energy of the envelope, the efficiency parameter and the change in the orbital energy during the CE phase, respectively.  $\alpha_{\text{CE}} = 1.0$  is taken in this work. The binding energy of the envelope is expressed by the following:

$$E_{\text{bind}} = -\frac{GM_1 M_{\text{en}}}{\lambda R_1} , \quad (2)$$

where  $M_1$ ,  $M_{\text{en}}$  and  $R_1$  are the total mass, envelope mass and radius of the primary star, respectively. The binding energy is related to the stars' mass and radius (with different evolutionary stages and metallicities). In the subroutine *comenv* of the updated code, we use the results of Wang et al. (2016) for the binding energy parameter  $\lambda$  of the donor envelope. Very recent CE study of Klencki et al. (2020) suggest that merger rates from previous works could be severely overestimated, especially at low metallicity due to the selected model of the binding energy parameter. Their results and discussions support the results of Wang et al. (2016). The orbital energy of the embedded binary is used to expel the envelope. If binaries cannot survive from the CE, they will merge into single stars, and cannot contribute to the ULX population. Binaries with stable mass transfer can avoid the CE, and the envelope of the donor stars will be reduced through Roche lobe overflow (RLOF). In the case of stable mass transfer, we simulate the binary orbital evolution by assuming that the ejected matter removes the specific orbital angular momentum of the accretor. For the wind mass loss, the prescriptions of Vink et al. (2001) were used for O and B stars in different stages (hot stars), and  $1.5 \times 10^{-4} \dot{M}_{\odot} \text{yr}^{-1}$  (Vink & de Koter 2002) is applied for luminous blue variable stars in the subroutine *mlwind* of the updated code (see the wind model 2 of Ablimit & Maeda (2018)). The prescription of the stellar wind mass losses in Hurley et al. (2000) are adopted for other type stars, such as Wolf-Rayet stars, cool red-giant-branch stars, etc.

The initial mass function of Kroupa et al. (1993) is utilized for the primary star in the Monte-Carlo sample generating subroutine *sample* of the code,

$$f(M_1) = \begin{cases} 0 & M_1/M_{\odot} < 0.1 \\ 0.29056(M_1/M_{\odot})^{-1.3} & 0.1 \leq M_1/M_{\odot} < 0.5 \\ 0.1557(M_1/M_{\odot})^{-2.2} & 0.5 \leq M_1/M_{\odot} < 1.0 \\ 0.1557(M_1/M_{\odot})^{-\alpha} & 1.0 \leq M_1/M_{\odot} \leq 150, \end{cases} \quad (3)$$

with  $\alpha = 2.7$  in this study. The secondary mass distribution follows the distribution of the initial mass ratio,

$$n(q) = \begin{cases} 0 & q > 1 \\ \mu q^{\nu} & 0 \leq q < 1, \end{cases} \quad (4)$$

where  $q = M_2/M_1$  and  $\mu$  is the normalization factor for the assumed power law distribution with index  $\nu$ . We consider a flat distribution ( $\nu = 0$  and  $n(q) = \text{constant}$ ) for the initial mass ratio distribution (IMRD). The distribution of the initial orbital separation,  $a_i$ , is (Davis et al. 2008),

$$n(a_i) = \begin{cases} 0 & a_i/R_\odot < 3 \text{ or } a_i/R_\odot > 10^6 \\ 0.078636(a_i/R_\odot)^{-1} & 3 \leq a_i/R_\odot \leq 10^6 . \end{cases} \quad (5)$$

The uniform (flat) initial eccentricity distribution is assumed in a range between 0 and 1.

Massive stars can evolve and become NSs through core-collapse SNe (CCSNe) (a star with initial mass  $\geq 10M_\odot$ ) or electron-capture SNe (a star with initial mass between  $8M_\odot \leq \leq 10M_\odot$ )<sup>1</sup>, and both SNe channels are considered in this work (e.g., Fryer et al. 2012). The SN explosion will impart a natal kick, and it causes eccentric orbit or disruption of the binary system if it is a strong kick. The kick velocities are assumed to obey Maxwellian distributions with a dispersion of  $\sigma = 40 \text{ km s}^{-1}$  (Dessart et al. 2006) for NSs formed from electron-capture SNe (ECSNe) and  $\sigma = 265 \text{ km s}^{-1}$  (Hobbs et al. 2005) for NSs formed from CCSNe. In both channels, the mass of NSs is limited between  $\sim 1.0$  and  $3.0 M_\odot$ , and the majority of NSs in our simulation results have masses in a range of  $\sim 1.0$  and  $2.0 M_\odot$ .

The accretion-induced collapse of an ONe WD is suggested as one important alternative formation way for NS binaries (e.g., Nomoto & Kondo 1991; Ablimit & Li 2015; Zhu et al. 2015; Ablimit 2019; Wang & Liu 2020). In this work, we study the contribution of the AIC channel to ULX pulsar binaries, and we employ the same method as Ablimit (2019) for the accretion process (e.g., retention efficiency of the transferred matter on the WD surface) of WD binaries. Although it was pointed out that the magnetic field of the WD may play a very important role in WD binary evolution (see Ablimit & Maeda 2019a, b; Ablimit 2019), we studied the non-magnetic case in this work. The default values of other physical parameters and other physical processes are the as same as described in Hurley et al. (2000, 2002).

The main evolution routes from close ZAMS + ZAMS binaries to NS + normal stars (including helium stars) binaries are very briefly described as follows: Route 1: a massive ZAMS star ( $\geq 10 M_\odot$ ) binary with a relatively unit mass ratio or relatively larger mass ratio starts their evolution, the more massive star evolves and first fills its Roche lobe (RL), then a stable or unstable RLOF mass transfer may occur. After the stable mass transfer ends or surviving from the CE, the primary massive one undergoes a CCSN and leaves a newborn

---

<sup>1</sup>Binary interaction could change the masses of the stars, thus the initial mass limits for leading CCSNe and ECSNe would be different compared to single stars. Knowing core masses of stars in binaries would be more useful to determine which of them go through ECSNe or CCSNe, and the relation of initial masses and core masses has been studied extensively (see recent works Sukhbold et al.(2016) and Woosely (2019) for more details).

NS, and forms an NS + normal star binary. Route 2: a massive ZAMS star (between 8 and 10  $M_{\odot}$ ) binary starts its evolution, and in other ways is similar to above evolution. There is an ECSN of the primary and forms an NS, then an NS + normal star binary begins its evolution. Route 3: an intermediate-mass ZAMS star (between 2 and 8  $M_{\odot}$ ) binary with a relatively bigger mass ratio. The more massive star evolves more and first fills its RL, then an unstable mass transfer may cause the CE phase. If the binary survives from the CE, the primary becomes a WD, then forms a WD + normal star binary. Later, the secondary fills its RL and starts the stable mass transfer. The WD accretes matter and grows in mass, and finally the WD collapses to form an NS when the WD’s mass reaches the Chandrasekhar limit mass (1.44  $M_{\odot}$  is adopted in this work), then an NS + normal star binary starts its evolution. In the section that showcases results, we provide the initial parameter distributions for these three routes.

## 2.2. Calculations for NS ULXs

The NS can be surrounded by matter which comes from the donor star, and an accretion disk can be formed around the NS. Matter moves from outside to inside of the disk, and the angular momentum transfers from inside to outside. The accretion model is crucial for the evolution of the system including the NS, and for observational signatures. If the mass from the donor transfers to the NS at a sub-Eddington rate, the formed accretion disk will be a thin disk, and it will become a thick disk when the mass transfer has a super-Eddington rate (Shakura & Sunyaev 1973). This accretion model is used for both RLOF and wind<sup>2</sup> mass accretion.

At the super-Eddington rate, the accretion luminosity is Eddington limited. The accretion luminosity can reach the Eddington luminosity at the spherization radius which is,

$$R_{\text{sph}} = \dot{M}_{\text{d}} \frac{GM_{\text{NS}}}{L_{\text{Edd}}}, \quad (6)$$

where  $\dot{M}_{\text{d}}$  and  $M_{\text{NS}}$  are the mass transfer rate from the donor star and mass of the NS, respectively.  $G$  is the gravitational constant. Outside  $R_{\text{sph}}$  the disk emits X-rays with

---

<sup>2</sup>For the wind accretion, we have adopted the Bondi & Hoyle (1944) accretion mechanism. The compact accretor captures a fraction of the mass lost from the donor by stellar wind. The prescription of Hurley et al. (2002) is applied for the wind accretion factor which determines the mean accretion rate into the disc around the compact accretor. The rest of the calculation is treated in the same way as for RLOF accretion.

luminosity the Eddington  $L_{\text{Edd}}$ ,

$$L_{\text{Edd}} = \eta \dot{M}_{\text{Edd}} c^2 = 2.6 \times 10^{38} \left( \frac{1}{1+X} \right) \left( \frac{M_{\text{NS}}}{M_{\odot}} \right) \text{erg s}^{-1}, \quad (7)$$

where  $c$  is the speed of light. The radiative efficiency<sup>3</sup> of accretion onto the NS is  $\eta = 0.1$  in this work. The Eddington limit for the mass accretion rate is  $\dot{M}_{\text{Edd}} = L_{\text{Edd}}/(\eta c^2)$  for an NS with a mass of  $M_{\text{NS}}$ .  $X$  is the hydrogen mass fraction in the donor envelope, and it is taken as 0.7 for H-rich donor stars and 0 for H-deficient donor stars in this work. Inside of the spherization radius ( $R_{\text{sph}}$ ), the disc is dominated by radiation pressure. Strong outflows begins and the accretion rate decreases linearly with radius. The mass accretion rate within  $R_{\text{sph}}$  at each point in the local disk follows the relation,

$$\dot{M}_{\text{Edd}}^L(R) = \dot{M}_{\text{d}} \frac{R}{R_{\text{sph}}}. \quad (8)$$

Because of the geometric collimation, one can see the source in directions within one of the cones, with an apparent (isotropic) X-ray luminosity. Given the mass transfer rate, we calculate the X-ray luminosity according to King (2008, 2009),

$$L_{\text{X}} = \frac{L_{\text{Edd}}}{b} (1 + \ln \dot{m}), \quad (9)$$

where the beaming factor  $b$  is,

$$b = \begin{cases} \frac{73}{\dot{m}^2} & \text{if } \dot{m} > 8.5 \\ 1 & \text{otherwise.} \end{cases} \quad (10)$$

where  $\dot{m} = \dot{M}_{\text{d}}/\dot{M}_{\text{Edd}}$ . In order to avoid the unphysical very high values when we approximate the beaming factor, the calculated accretion (apparent) luminosity is limited by  $10^{39} \leq L_{\text{X}} \leq 10^{44} \text{erg s}^{-1}$ .

In the accreting NS binaries, NSs can be easily spun up to be (millisecond) pulsars during the evolution processes by mass accretion, and the spin rates of the recycled pulsars would be slower if the companion stars are more massive and/or giant stars due to the shorter timescale of the mass-transfer (X-ray) phase of massive and/or giant stars (e.g., Tauris, Langer & Kramer 2012). For a slow or non-rotator newborn NS, the amount of accreted mass needed to spin up as a pulsar has been studied and discussed by Tauris, Langer & Kramer (2012). An NS with a typical mass of  $1.4 M_{\odot}$  can spin up to 50 milliseconds from

---

<sup>3</sup>Note that the radiative efficiency would vary according to the NS mass.



rest if it accretes only a small amount of mass ( $10^{-3} M_{\odot}$ ) (see the equations and discussions of Tauris, Langer & Kramer (2012) for more details). Observed spin periods of ULXs pulsars (see Table 1) are at the level of level which naturally can be achieved by the mass-transfer (X-ray) phases of ULXs. In our calculation, most of the NSs in ULXs have pulse periods distributed between  $\sim 0.3$  and 10 seconds. Thus, we assume all NSs in ULX binaries can be pulsars, and we do not trace after the spin period evolution of the NS in this study. We investigate the formation of ULX binaries, and try to explain the observed orbital periods, apparent luminosities and indicated masses of known ULX pulsar binaries.

### 3. Results

We simulate evolutions of MS-MS binaries which evolve toward ULX pulsar binaries with different types of companion stars, and we also explore the final outcomes of ULX pulsar binaries. In this work, the type of non-degenerate companion stars (its mass is  $M_d$ ) are defined as follows: the stars at the central hydrogen burning stage are assumed as the MS stars; cases that finished all central hydrogen burning are considered as evolved stars; The evolved normal stars include sub-giant stars (hydrogen-rich Hertzsprung gap stars), and giant branch stars (red giant stars, core helium burning stars, etc.); stars with masses  $< 2 M_{\odot}$  are low-mass stars; stars with masses  $2 \leq M_d < 8 M_{\odot}$  are intermediate-mass stars; stars with masses  $\geq 8 M_{\odot}$  are massive stars; Rapidly rotating B-type stars are categorized as Be stars, and rotation speed of Be stars generally reaches nearly their Keplerian limits. If spin angular velocities of stars are close to their critical spin angular velocities ( $\frac{\omega}{\omega_{cr}} > 0.85$ ), they are selected as Be stars; Note that Be stars and other slow rotator stars with  $\frac{\omega}{\omega_{cr}} \leq 0.85$  (MS and evolved stars) are seen as normal stars; Stars are categorized as Helium stars if their hydrogen-rich envelope are stripped away by the binary interactions, and He MS, He-rich Hertzsprung gap and He giant stars are considered as He stars in this work.

#### 3.1. Mass, orbital period and luminosity profiles of ULX pulsar binaries

In this subsection, we show calculated orbital periods ( $P_{orb}$ ), masses and accretion luminosities of ULX pulsar binaries, and compare our results with those of observed ULX pulsar binaries. In Figure 1, the red triangles represent the data of observed ULX pulsar sources, and the other colors and symbols show the simulated ULXs with different type of companions. Because the observational mass predictions have uncertain values (see Table 1, and see Section 1 for discussion), we take values within the observational indications for companions' masses and a few uncertain orbital periods of seven observed ULXs, such as  $M_d = 10 M_{\odot}$

and  $P_{\text{orb}} = 380$  days for NGC 300 ULX-1;  $M_{\text{d}} = 6.0 M_{\odot}$  and  $P_{\text{orb}} = 6$  days for the source NGC 1313 X-2;  $M_{\text{d}} = 5.2 M_{\odot}$  for the source M82 X-2;  $M_{\text{d}} = 20 M_{\odot}$  for the source NGC 7793 P13;  $M_{\text{d}} = 4.0 M_{\odot}$  for the source NGC 5907 ULX-1;  $M_{\text{d}} = 3.7 M_{\odot}$  for the source SMC X-3;  $M_{\text{d}} = 6.0 M_{\odot}$  for the source M51 ULX-1. The donor mass and orbital period distributions from our calculations show that Be stars, massive stars and intermediate mass stars are more likely companion stars to ULXs as their values match the observationally indicated values of seven ULX pulsar binaries. The luminosity distributions in Figure 2 demonstrate that NS binaries with different types stars can be higher than  $L_{\text{X}} \geq 10^{39} \text{ erg s}^{-1}$ , and at least 80% of them have luminosities distributed in  $10^{39} \leq L_{\text{X}} \leq 10^{41} \text{ erg s}^{-1}$ . The apparent luminosities of all nine known pulsar ULXs (Table 1) can be reproduced by the simulation.

Although binaries with low-mass stars can be companions to ULX pulsar binaries, the derived masses and most orbital periods of low-mass stars are not consistent with currently available observational mass indications of seven sources. He stars can also contribute to ULX pulsar systems, however, the mass of He stars in ULX systems is mainly distributed between  $0.6$  and  $2.8 M_{\odot}$  which are lower than observationally predicted ones (wider than the mass range from Wiktorowicz et al.(2019)). The systems with a massive helium star are hardly produced because of a combination of relatively low birthrates, short mass transfer durations, and low detection possibilities (due to the beaming effect). ULXs with He stars have age from 18 Myr to 210 Myr. The orbital period distribution of ULX pulsar binaries with He stars has a peak at 0.1 day, and the longest one is up to a few hundred days. The systems containing NSs and He stars are also promising multi-messenger sources for the upcoming electromagnetic and GW facilities (e.g., Götzberg et al. 2020), but this is not the focus of this work. We discuss normal star companions in more details below.

Figure 3 shows the initial masses and initial orbital period distributions of progenitors of ULX pulsar binaries with normal star donors. Distributions are basically consistent with results of previous BPS studies (e.g., Fragos et al.2015). 91.5% of NSs in ULX systems with normal star companions are born through CCSNe, 4.5% of NSs in ULXs are formed through the AIC of massive WDs, and 4.0% of NSs in ULX binaries are produced through electron-capture SNe (see the above section for more discussions of the three routes). The main properties of ULX pulsar binaries are shown in Figure 4. Donor mass distributions of pulsar ULXs show that 8.9% of pulsar ULXs have low mass companions while 91.1% of them have intermediate or massive star companions. The majority of NS ULXs were believed to contain red giant companions with typical masses around  $1 M_{\odot}$  by Wiktorowicz et al.(2017). However, masses indicated by recent observations for seven known ULX pulsar systems (see Table 1) imply that Be stars, massive stars and/or intermediate-mass stars could be companion stars in these pulsar binaries, which are consistent with what our BPS simulations find. Most ULXs in this work have orbital periods between  $\sim 1$  and 10 days

(Figure 4), and this also supports the statements given by BPS results of Fragos et al.(2015) and detailed binary evolution results of Misra et al.(2020). ULX binaries with Be stars have age between 12 Myr and 217 Myr in our calculation, but the ages of other normal stars are mainly distributed between 18 Myr and 1 Gyr (up to several Gyr).

Formation of ULX pulsar binaries containing Be star donors is more common in our simulation. Their orbital periods are distributed from  $> 1$  day to  $\sim 1000$  days, and Be star masses have a range of  $2.5 M_{\odot} - 30 M_{\odot}$ . These properties cover the observationally indicated masses and orbital periods of all seven ULX pulsar sources displayed in Table 1 and Figure 1 (at least covering five possible candidates known as Be ULXs which exhibit transient phases of X-ray emission, such as NGC 300 ULX1 (Binder et al. 2016) and SMC X-3 (Townsend et al. 2017)). One of the main features of a Be star is fast rotation which is considered in this work by including the mass transfer and tidal effect, and binary interactions like the mass transfer and tidal effect have been suggested as possible mechanisms for fast rotation of the star and formation of ULXs (e.g., Ablimit & Lü 2013). An excretion disk would be formed around Be stars due to the fast rotational velocities of Be stars. NSs in most NS-Be star binaries (Reig 2011) accrete matter when they pass through or are close to the Be star’s circumstellar disc. Theoretical models usually assume that a Be star is just a rapid rotator, and it is very difficult to include the Be disk in the 1D modeling. There are some important details in the formation of circumstellar discs around Be stars and origin of different types of outbursts in galactic and extragalactic Be stars, which need further investigations (Lee, Osaki & Saio 1991; Negueruela et al. 2001; Negueruela & Okazaki 2001; Martin et al. 2014). These physical processes are out of the scope of this work.

### 3.2. Rates of the ULX pulsar binary

The birth rate ( $R_B$ ) of a type of binary can be calculated by the following equation,

$$R_B = f_{\text{bin}} \times \eta_{\text{SFR}} \times \frac{N}{M_{\text{total}}}, \quad (11)$$

where  $N$  is the total number of a specific binary types, and  $M_{\text{total}}$  is the total mass of all stellar systems.  $\eta_{\text{SFR}}$  is the star formation rate.  $f_{\text{bin}}$  is a fraction of binaries in all stellar systems, which is  $f_{\text{bin}} = \frac{N_{\text{bin}}}{N_{\text{bin}} + N_{\text{single}}}$ .

In Table 2, we show the formation rates of ULX pulsar binaries per  $10^6 M_{\odot}$  of created stars in the simulation with different donors. If we assume a constant star formation rate of  $\eta_{\text{SFR}} = 3 M_{\odot} \text{ yr}^{-1}$  and binarity of  $f_{\text{bin}} = 0.7$ , we obtain that the birth rates of ULX pulsar binaries with normal stars and He stars are  $\sim 1.83 \times 10^{-4} \text{ yr}^{-1}$  and  $\sim 3.36 \times 10^{-5} \text{ yr}^{-1}$  at the

solar metallicity case, respectively. We also calculated the formation rates for the population II stars (low metallicity case), and the rates become higher with the case of  $Z = 0.001$ . Be stars are main donors for ULXs in our calculation, and the evolved stars (HG or/and giant branch stars) are much less than MS donors. Only among low-mass donors, the evolved stars are comparable with low mass MS stars, while it is just  $\sim 4.0\%$  and  $3.7\%$  among intermediate and high mass donors (MS donors are significantly more), respectively. Wiktorowicz et al. (2017, 2019) only considered RLOF mass transfer case in their study, but they did not include the wind-fed mass transfer (which plays an important role in massive star binary evolution), thus it may cause an underestimation of the fraction of high mass donors in ULXs (about 1%). A recent ULX observational result of López et al. (2020) indicates that the fraction of giant massive stars could be around  $4 \pm 2\%$  (note that they did not categorize the accretor of ULXs in their observational result). This is higher than what Wiktorowicz et al. (2017) find, but it is supported by our results. We also show the rate evolutions of ULXs with the constant star formation model and a single burst star formation model in Figure 5. The large number of ULX pulsar binaries at solar metallicity needs a shorter timescale than that of the low metallicity case, and they all have a peak in the first  $< 100$  Myr (a significant number of NS ULXs have their ULX phases during the post MS expansion of their donors at low metallicity). Our results suggest the solar metallicity condition for producing current observational results of pulsar ULXs.

### 3.3. Evolution of ULX pulsar binaries to Pulsar-NS and Pulsar-WD systems for the LISA detector

Except for ULXs with very low mass donors, ULXs with intermediate-mass donors and He stars naturally evolve to form pulsar - WD binaries in the Hubble time, and they have a large fraction of whole ULXs. A pulsar-NS system also can be expected from ULXs with massive stars. From the current understanding of binary evolution, they also may evolve into the CE phase during the evolution of ULX pulsar binaries, and they will form double compact objects in close orbits if they survive from the CE, otherwise they will merge inside the CE and become one object. The connections between ULXs and double compact star objects (DCOs) can potentially be important to understand the origin of merging DCOs detected by LIGO. We analyze our BPS results with the solar metallicity case and try to find those connections.

In this work, we find that pulsar ULXs would become pulsar-WD and pulsar-NS systems (no other DCOs). After a pulsar-WD binary formed in a very short orbit, the WD can fill its Roche lobe and the mass transfer may proceed. The merger or an ultra-compact X-ray

binary (UCXB; e.g., Heinke et al. 2013; Lü et al. 2017) can be expected depending on the stability of the RLOF mass transfer. Because we derived similar merger rates with different models, we assume the final stage of a pulsar-WD system will be a merger through emitting GW signals.

The orbital motion of a pulsar-WD or pulsar-NS binary system can lead to GW emission and spiral-in of the system. The continuous energy loss through GW emission (according to general relativity) will merge the two objects at the final stage of the inspiraling process. The timescale (Peters & Mathews 1963; Peters 1964; Lorimer 2008) of the merging process is expressed as,

$$t = 9.88 \times 10^6 \left(\frac{P_{\text{orb}}}{1 \text{ hr}}\right)^{8/3} \left(\frac{\mu}{1 M_{\odot}}\right)^{-1} \left(\frac{M}{1 M_{\odot}}\right)^{-2/3} \text{ yr}, \quad (12)$$

where  $\mu = M_1 M_2 / (M_1 + M_2)$  and  $M = M_1 + M_2$  are the reduced mass and total mass of the system ( $M_1$  and  $M_2$  are the masses of two objects in a binary system), respectively.

The continuous GW emission takes away orbital angular momentum and shrinks the orbit, and the GW strain will increase with time during the merging process. If the distance of the binary system with respect to us is  $d$ , then the strain amplitude of the GW can be expressed as (Peters & Mathews 1963)

$$h = 5.1 \times 10^{-23} \left(\frac{P_{\text{orb}}}{1 \text{ hr}}\right)^{-2/3} \left(\frac{M_{\text{ch}}}{1 M_{\odot}}\right)^{5/3} \left(\frac{d}{10 \text{ kpc}}\right)^{-1}, \quad (13)$$

where  $M_{\text{ch}} = (M_1 M_2)^{3/5} / (M_1 + M_2)^{1/5}$  is the chirp mass. The GW frequency  $f$  is twice the orbital motion frequency.

From the results of the BPS simulation, we derive that rates of NS-WD and NS-NS systems that can merge in a Hubble time are  $1.28 \times 10^{-4} M_{\odot}^{-1}$  and  $4.34 \times 10^{-5} M_{\odot}^{-1}$ , respectively. If a constant star formation rate of  $\eta_{\text{SFR}} = 3 M_{\odot} \text{ yr}^{-1}$  and binarity of  $f_{\text{bin}} = 0.7$  are adopted, the merger rate of NS-WD and NS-NS systems that can merge in a Hubble time are  $2.69 \times 10^{-4} \text{ yr}^{-1}$  ( $\sim 2690 \text{ Gpc}^{-3} \text{ yr}^{-1}$ ) and  $0.91 \times 10^{-4} \text{ yr}^{-1}$  ( $\sim 910 \text{ Gpc}^{-3} \text{ yr}^{-1}$ ) in Milky Way-like galaxies, respectively. The rate of double NS merger in this work is consistent with the observationally inferred rate by LIGO (250 - 2810  $\text{Gpc}^{-3} \text{ yr}^{-1}$ ) (Abbott et al. 2020). Among them, at least  $\sim 19.2\%$  of NS-WD merger signal and  $\sim 7.8\%$  NS-NS merger signal can be detected by LISA.  $\sim 41\%$  of all the NS-WD population is pulsar-WD systems that evolved from ULX pulsar binaries, while  $\sim 4.2\%$  of those NS-NS systems is pulsar-NS systems formed from ULX pulsar binaries (Figure 6).  $\sim 13\%$  of ULXs with He stars and  $\sim 87\%$  of ULXs with normal stars contribute to the pulsar-WD GW sources, and all pulsar-NSs evolved from ULXs with normal stars. From the whole NS-WD and NS-NS populations that merge

in the Hubble time, we find that contributions of pulsar-WD and pulsar-NS systems from ULX pulsar channels for LISA are  $\sim 10.5\%$  and  $\sim 1.0\%$  (as shown in Figure 6), respectively. Note that the finite size of the Monte Carlo simulation gives a statistical fluctuation. With different BPS models (Ablimit et al. 2016; Ablimit & Maeda 2018), the relative statistical error is estimated to be  $\sim 5\%$ – $35\%$ .

#### 4. Discussion and Conclusion

The observational results of ULXs are increasing, and the properties of known pulsar ULXs need further investigations. We simulated a large number of binary evolutions, and analyzed physical processes. In the primordial binary evolution, we adopted a non-conservative and rotation-dependent mass transfer model (numerically calculated critical mass ratio) which allows most primordial systems to have stable mass transfer, and this makes more NSs have relatively higher mass donors (most of them are intermediate mass donors). Thus, we have a few percent higher high mass donor ULXs compared to previous works, and have significantly more intermediate mass ULXs as shown in the results section. Formation of NS ULXs with normal stars in this work is less dependent on the ejection of CE compared to previous works. The mass transfer model and metallicity have important roles in the formation and evolution of ULXs. The later evolution of more NS + normal star binaries experience the CE phase, and a more reliable model of binding energy for the CE evolution is adopted in the work. The main results can be concluded as follows:

1. Our BPS simulations tend to have more pulsar ULXs with Be stars and intermediate mass donors. The observationally indicated properties of seven known pulsar ULXs can be fully reproduced by the combined results of Be and intermediate mass ULXs. Few known ULXs also can be formed with high mass donors. NS ULXs with He star or low mass donors are not consistent with current observations of seven pulsar ULXs, although they have obvious contributions to NS ULXs in the simulation results. The rate (number) of pulsar ULXs can be higher with the population II ( $Z = 0.001$ ) case than that of the population I ( $Z = 0.02$ ) case.
2. The AIC route has 4.5% contribution to the NS ULXs. 4.0% of NSs in ULXs are formed through ECSNe, while 91.5% of NSs in ULXs are born with CCSNe. The fraction of pulsar ULXs with MS donors is significantly larger than that of ULXs with evolved donors. The fractions of evolved hydrogen-rich low, intermediate and high mass donors in the whole normal star donors are 3.3%, 3.5% and 3.2%, respectively.
3. We do not find pulsar - BH systems evolved from pulsar ULXs who can merge in the

Hubble time. We discover that pulsar-NS and pulsar-WD systems from ULXs have  $\sim 4.2\%$  and  $41\%$  contributions to the whole NS-NS and NS-WD systems which merge in a Hubble time. Pulsar-NS systems evolved from ULXs with normal stars, while  $\sim 13\%$  ULXs with He stars and  $\sim 87\%$  ULXs with normal stars evolved to form pulsar-WD binaries which can merge in the age of the Universe. Among the all detectable NS-NS and NS-WD systems for the LISA detector,  $\sim 11\%$  and  $40\%$  are pulsar-NS and pulsar-WD systems that evolved from ULXs. The Monte Carlo simulation uncertainties with different BSP models should be considered when dealing with these contributions.

This work was supported by the National Natural Science Foundation of China, project No. 11863005. The LAMOST FELLOWSHIP is supported by Special Funding for Advanced Users, budgeted and administrated by Center for Astronomical Mega-Science, Chinese Academy of Sciences.

## REFERENCES

- Abbott, B. P., Abbott, R., Abbott, T. D., LIGO collabortaion, et al., 2020, ApJL, 892, L3
- Ablimit, I. & Li, X.-D., 2015, ApJ, 800, 98
- Ablimit, I. Maeda, K. & Li, X.-D., 2016, ApJ, 826, 53
- Ablimit, I. & Maeda, K., 2018, ApJ, 866, 151
- Ablimit, I. & Lü, GuoLiang, 2013, SCPMA, 56, 663
- Ablimit, I. & Maeda, K., 2019a, ApJ, 871, 31
- Ablimit, I. & Maeda, K., 2019b, ApJ, 885, 99
- Ablimit, I., 2019, ApJ, 881, 72
- Bachetti, M., et al., 2014, Nature, 514, 202
- Binder, B., Williams, B. F., Kong, A. K. H., 2016, MNRAS, 457, 1636
- Bondi, H. & Hoyle, F., 1944, MNRAS, 104, 273
- Brightman, M., et al., 2018, NatAs, 2, 312
- Brightman, M., Balokovic, M., Koss, M., et al., 2018b, ApJ, 867, 110

- Brightman, M., Harrison, F. A., Bachetti, M., et al., 2019, *ApJ*, 873, 115
- Colbert, E. J. M., Mushotzky, R. F., 1999, *ApJ*, 519, 89
- Carpano, S., Haberl, F., Maitra, C., et al., 2018, *MNRAS*, 476, L45
- Chandra, A. D., Roy, J., Agrawal, P. C. & Choudhury, M., 2020, *MNRAS*, 495, 2664
- Dall’Osso S., Perna R., Stella L., 2015, *MNRAS*, 449, 2144
- Davis, P. J., Kolb, U., Willems, B., Gnsicke, B. T., 2008, *MNRAS*, 389, 1563
- de Mink, S. E., Langer, N., Izzard, R. G., Sana, H., & de Koter, A. 2013, *ApJ*, 764, 166
- de Mink, S. E., Pols, O. R., Langer, N., & Izzard, R. G. 2009, *A&A*, 507, L1
- Dessart, L., Burrows, A., Ott, C. D., et al. 2006, *ApJ*, 644, 1063
- Doroshenko V., Tsygankov S., Santangelo A., 2018, *A&A*, 613, A19
- Finke, J. D., Razzaque, S., 2017, *MNRAS*, 472, 3683
- Fabbiano, G., 1989, *ARA&A*, 27, 87
- Feng, H., Soria, R., 2011, *New Astronomy Reviews*, 55, 166
- Fürst, F., Walton, D. J., Harrison, F. A., et al., 2016, *ApJ*, 831, L14
- Fürst, F., Walton, D. J., Heida, M. et al., 2018, *A&A*, 616, A186
- Fragos, T., Linden, T., Kalogera, V., & Sklias, P. 2015, *ApJ*, 802, L5
- Fryer, C. L., Belczynski, K., Wiktorowicz, G., et al. 2012, *ApJ*, 749, 91
- Götberg, Y., Korol, V., Lamberts, A. et al., 2020, arXiv:2006.07382
- Heinke, C. O., Ivanova, N., Engel, M. C., et al. 2013, *ApJ*, 768, 184
- Heida, M., Harrison, F. A., Brightman, M., Fürst F., SternD., Walton D. J., 2019, *ApJ*, 871, 231
- Heida, M., et al., 2019, *ApJL*, 883, L34
- Herold, H., 1979, *PhRvD*, 19, 2868
- Hobbs, G., Lorimer, D. R., Lyne, A. G., & Kramer, M. 2005, *MNRAS*, 360, 974
- Hurley, J. R., Pols, O. R., Tout, C. A., 2000, *MNRAS*, 315, 543
- Hurley, J. R., Tout, C. A., Pols, O. R., 2002, *MNRAS*, 329, 897



- Israel, G. L., Papitto, A., Esposito, P., et al., 2017a, *Science*, 355, 817
- Israel, G. L., Papitto, A., Esposito, P., et al., 2017, *MNRAS*, 466, L48
- Kaaret, P., Feng, H., & Roberts, T. P. 2017, *ARA&A*, 55, 303
- King, A. R., 2008, *MNRAS*, 385, L113
- King, A. R. 2009, *MNRAS*, 393, L41
- King, A., Lasota, J.-P., 2019, *MNRAS*, 485, 3588
- King, A., Lasota, J.-P., 2020, arXiv arXiv:2003.14019
- King, A. R., Davies, M. B., Ward, M. J., et al. 2001, *ApJ*, 552, L109
- Klencki, J., Nelemans, G., Istrate, A.-G. & Chruslinska, M., 2020, arXiv:2006.11286
- Kluźniak, W., Lasota, J. P., 2015, *MNRAS*, 448, L43
- Kroupa, P., Tout, C. A., Gilmore, G., 1993, *MNRAS*, 262, 545
- Lee U., Osaki Y. & Saio H., 1991, *MNRAS*, 250, 432
- López, K. M., Heida, M., Jonker, P. G., et al., 2020, arXiv: 2006.02795
- Lorimer, D. R. 2008, *LRR*, 11, 8
- Lü, GuoLiang, Zhu, C.-H., Wang, Z.-j., Iminniyaz, H., 2017, *ApJ*, 847, 62
- Martin R. G., Nixon C., Armitage P. J., Lubow S. H. & Price D. J., 2014, *ApJ*, 790, L34
- Misra, D., Fragos, T., Tauris, T. M., Zapartas, E. & Aguilera-Dena, D. R. 2020, arXiv::2004.01205
- Mushtukov, A. A., Suleimanov, V. F., Tsygankov, S. S., et al. 2015, *MNRAS*, 454, 2539
- Marchant, P., Langer, N., Podsiadlowski, P., et al. 2017, *A&A*, 604, A55
- Negueruela I., Okazaki A. T., 2001, *A&A*, 369, 108
- Negueruela I., Okazaki A. T., Fabregat J., Coe M. J., Munari U., Tomov T., 2001, *A&A*, 369, 117
- Nomoto, K., Kondo, Y., 1991, *ApJ*, 367, L19
- Shakura, N. I., Sunyaev, R. A., 1973, *A&A*, 24, 337
- Packet, W., 1981, *A&A*, 102, 17

- Paxton, B., Marchant, P., Schwab, J., et al., 2015, *ApJS*, 220, 15
- Petrovic, J., Langer, N., & van der Hucht, K. A., 2005, *A&A*, 435, 1013
- Peters, P. C. 1964, *PhRv*, 136, B1224
- Peters, P. C., & Mathews, J. 1963, *PhRv*, 131, 435
- Poutanen, J., Lipunova, G., Fabrika, S., et al. 2007, *MNRAS*, 377, 1187
- Rajoelimanana, A. F., Charles, P. A., Udalski A., 2011, *The Astronomer’s Telegram*, 3154
- Reig, P. 2011, *Ap&SS*, 332, 1
- Rodríguez Castillo, G. A., et al., 2019, arXiv arXiv:1906.04791
- Sathyaprakash, R., Roberts, T. P., Walton, D. J., et al., 2019, *MNRAS*, L104
- Shao, Y. & Li, X.-D., 2015, *ApJ*, 802, 131
- Sukhbold, T., Ertl, T., Woosley, S. E., et al., 2016, *ApJ*, 821, 38
- Tauris, T. M., Langer, N. & Kramer, M. 2012, *MNRAS*, 425, 1601
- Tsygankov, S. S., Doroshenko, V., Lutovinov, A. A., et al., 2017, *A&A* 605, A39
- Townsend, L. J., Kennea, J. A., Coe M. J., et al., 2017, *MNRAS*, 471, 3878
- Vasilopoulos, G., Ray, P. S., Gendreau, K. C., et al., 2020, *MNRAS*, 494, 5350
- Vink, J. S., de Koter, A., & Lamers, H. J. G. L. M. 2001, *A&A*, 369, 574
- Vink, J. S., & de Koter, A. 2002, *A&A*, 393, 543
- Wang, B., & Liu, D., 2020, *RAA*, 20, 133
- Wang, C., Jia, K., & Li, X.-D. 2016, *RAA*, 16, 126
- Webbink, R. F. 1984, *ApJ*, 277, 35
- Wiktorowicz, G., Sobolewska M., Lasota J.-P. & Belczynski, K. 2017, *ApJ*, 846, 17
- Wiktorowicz, G., Lasota, J.-P., Middleton, M., & Belczynski, K. 2019, *ApJ*, 875,53
- Walton, D. J., Furst, F., Bachetti, M. et al., 2016, *ApJ*, 827, L13
- Woosely, S. E. 2019, *ApJ*, 878, 49
- Zhu, C.-H., Lü, G.-L., & Wang, Z. 2015, *MNRAS*, 454, 1725

Table 1: Observed properties of ULX pulsars

ULX pulsars	$L_x$ (erg s $^{-1}$ )	$P_s$ (s)	$P_{orb}$ (d)	$M_2$ ( $M_\odot$ )
NGC7793 P13 <sup>1,2,3</sup>	$5 \times 10^{39}$	0.42	64.0	18.0-23.0
NGC5907 ULX-1 <sup>4,5,6</sup>	$\sim 10^{41}$	1.137	5.3	2.0-6.0
M82 X-2 <sup>7,8</sup>	$1.8 \times 10^{40}$	1.37	2.52	$\geq 5.2$
NGC1313 X-2 <sup>9</sup>	$1.5 \times 10^{40}$	1.46	$< 6$	$\leq 12$
M51 ULX-7 <sup>10,11,12</sup>	$7.1 \times 10^{39}$	2.8	2.0	$\geq 8$
SMC X-3 <sup>13,14,15</sup>	$2.5 \times 10^{39}$	7.77	44.92	$\geq 3.7$
Swift J0243.6+6124 <sup>16,17</sup>	$1.8 \times 10^{39}$	9.86	28.3	–
NGC300 ULX-1 <sup>18</sup>	$4.7 \times 10^{39}$	31.6	$> 300$	$\geq 8 - 10$
NGC 2403 ULX <sup>19</sup>	$1.2 \times 10^{39}$	$\sim 18$	60-100 (?)	–

1, Fürst et al. (2016); 2, Israel et al. (2017b); 3, Fürst et al. (2018); 4, Walton et al.(2016); 5, Heida et al.(2019); 6, Israel et al. (2017a); 7, Bachetti et al. (2014); 8, Brightman et al. (2019); 9, Sathyaprakash et al. (2019); 10, Rodríguez Castillo, et al. (2019); 11, Brightman et al.(2018b) ; 12, Vasilopoulos et al. (2020); 13, Doroshenko, Tsygankov & Santangelo.(2018); 14, Townsend et al.(2017); 15, Rajoelimanana et al.(2011); 16, Townsend et al. (2017); 17, Doroshenko et al.(2018); 18, Carpano et al. (2018); 19, Tsygankov et al. (2017). Note: There is new source recently found, which is RX J0209.6-7427 (see Chandra et al. 2020).

Table 2: Formation rates of ULXs pulsar binaries (with different type of companions) per  $10^6 M_{\odot}$  of created stars for the simulation

Companion Type	Rate with $Z = 0.02$	Rate with $Z = 0.001$
LM MS	5.4	9.3
LM evolved	3.3	5.2
IM MS	22.9	28.0
IM evolved	3.5	7.3
HM MS	10.2	18.8
HM evolved	3.2	4.2
Be star	39.0	61.6
He star	16.0	45.8

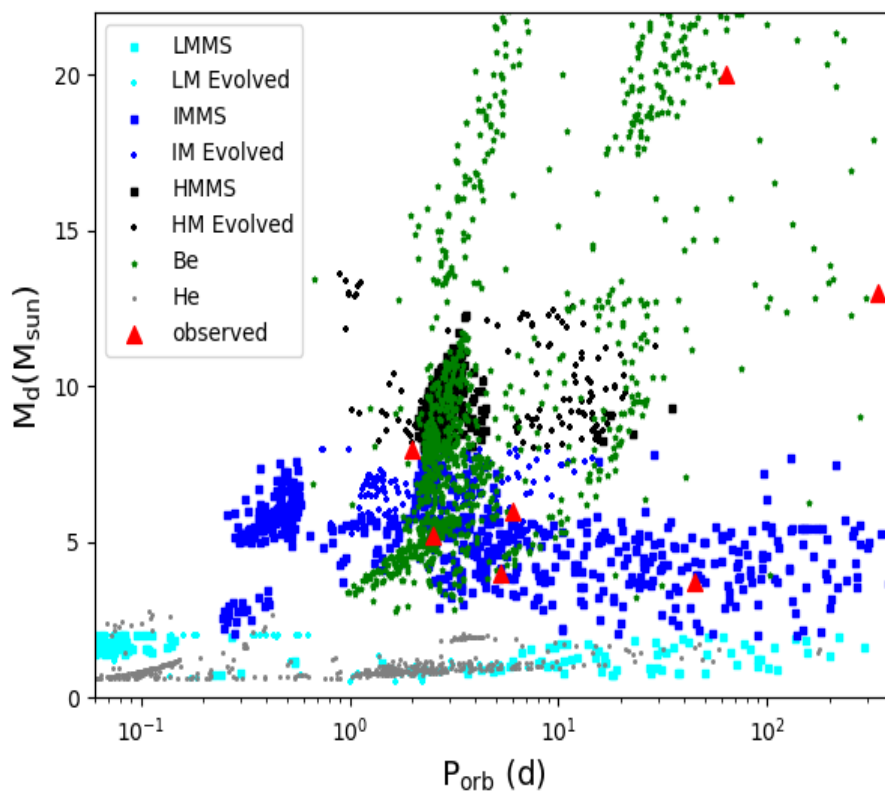


Fig. 1.— The distributions of the orbital periods and companion stars’ mass for ULX pulsar binaries. Red triangles are observed sources (Table 1). ULX pulsar binaries from our results with Be star companions, He Star, low-mass star (LM, including MS & evolved), intermediate-mass star (IM, including MS & evolved), and high mass star (HM, including MS & evolved) companions are shown, respectively.

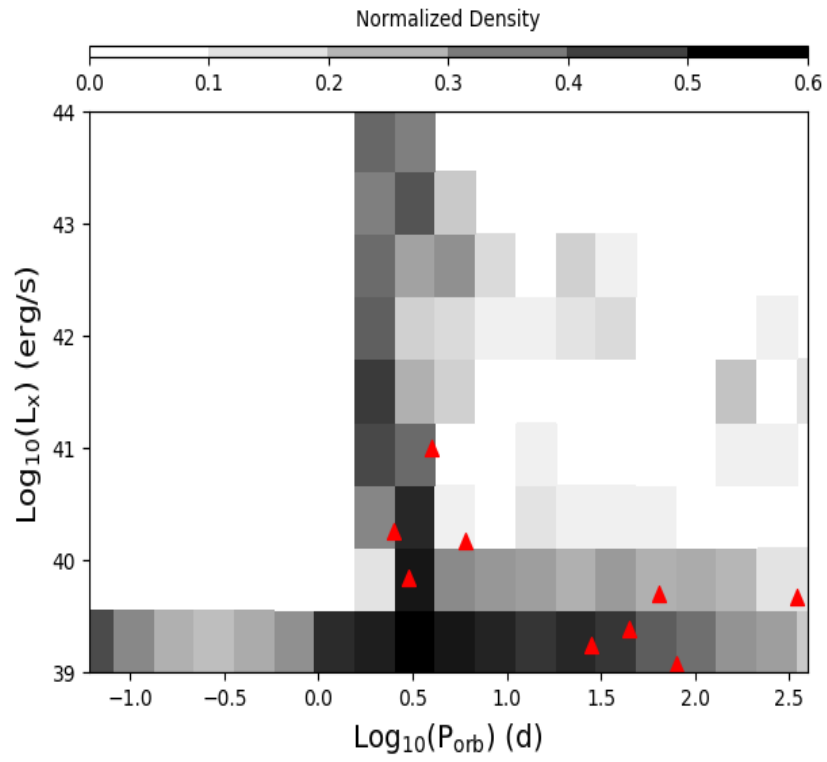


Fig. 2.— The distributions of the orbital periods and accretion (apparent) luminosities for ULX pulsar binaries. Red triangles are observed pulsar ULX sources.

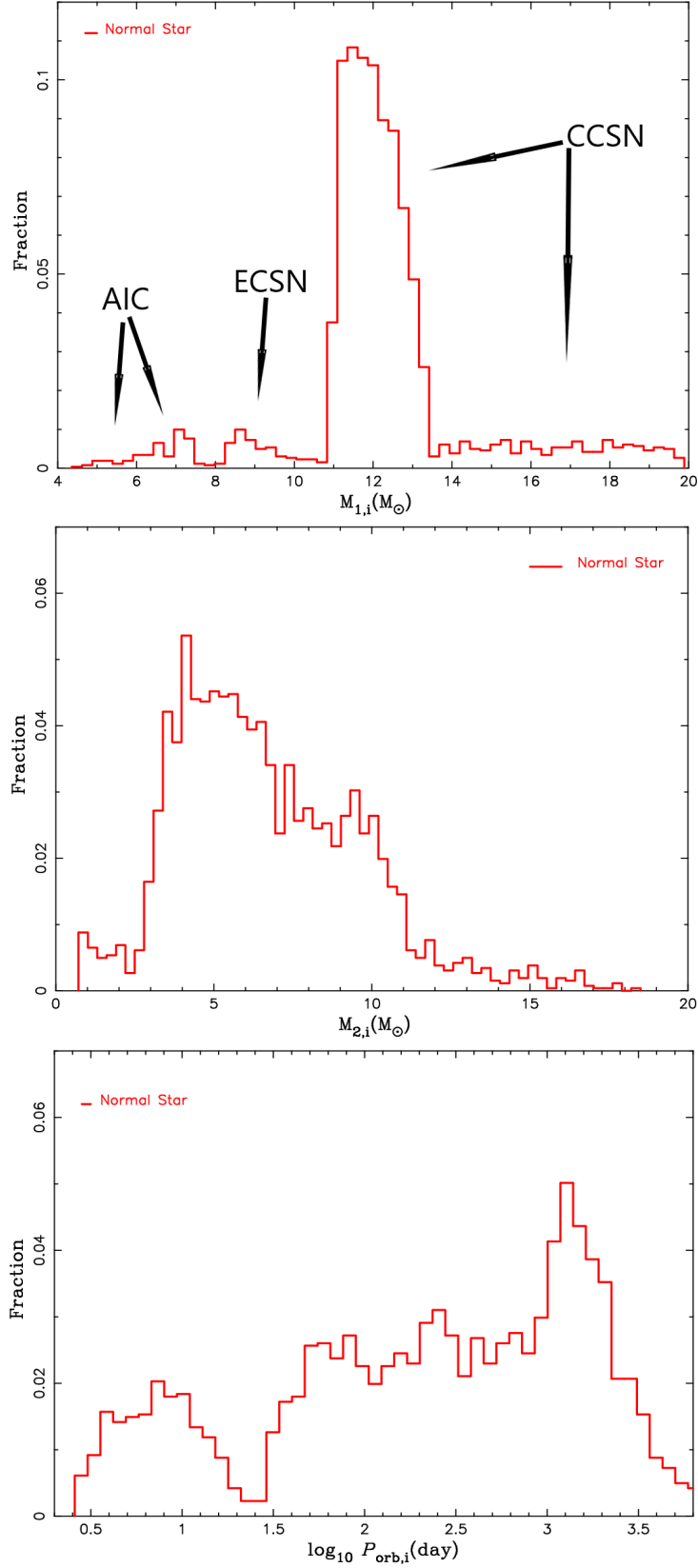


Fig. 3.— The distributions of progenitors of ULX pulsar binaries at the beginning. The initial masses of primary & secondary stars, and initial orbital periods are shown in upper, middle and lower panels, respectively.

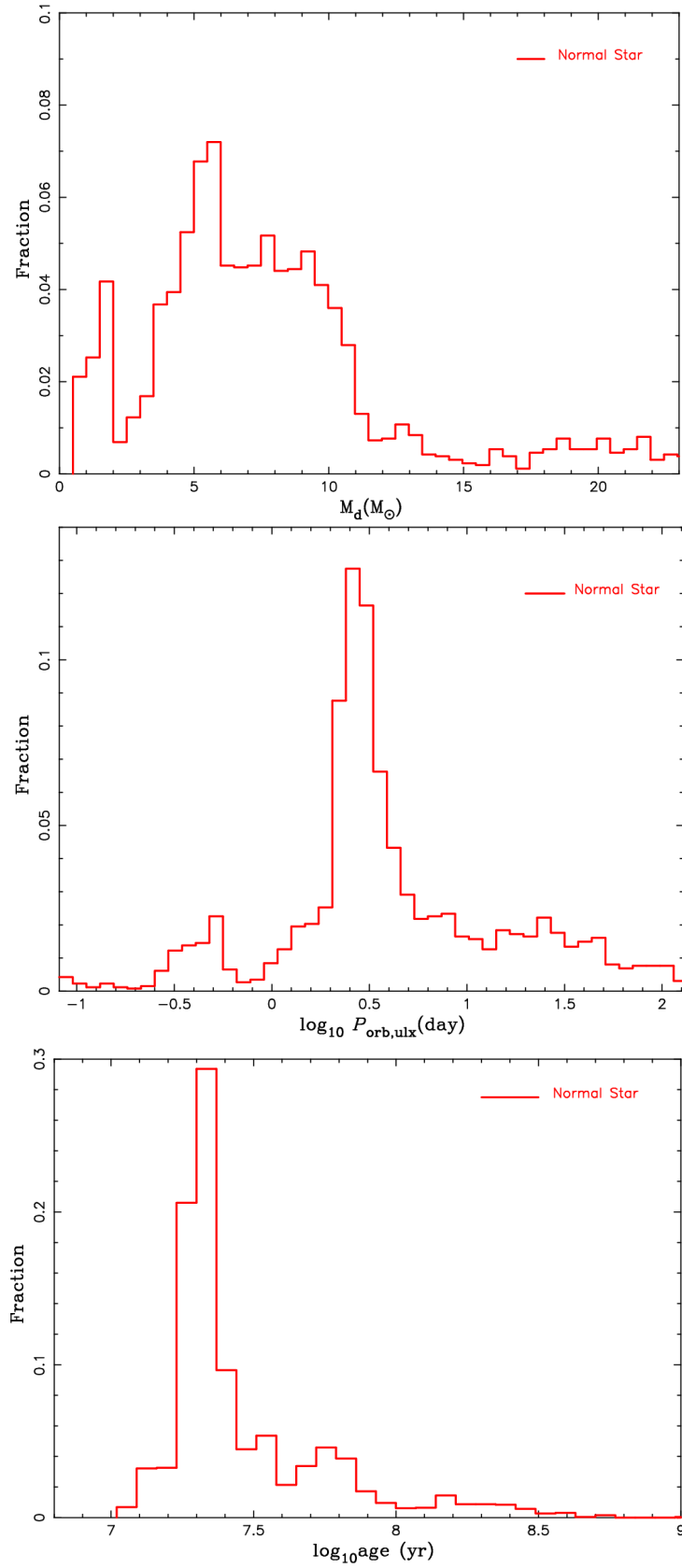


Fig. 4.— The distributions of the donor mass, orbital periods and ages of ULX pulsar binaries have given in upper, middle and lower panels, respectively.



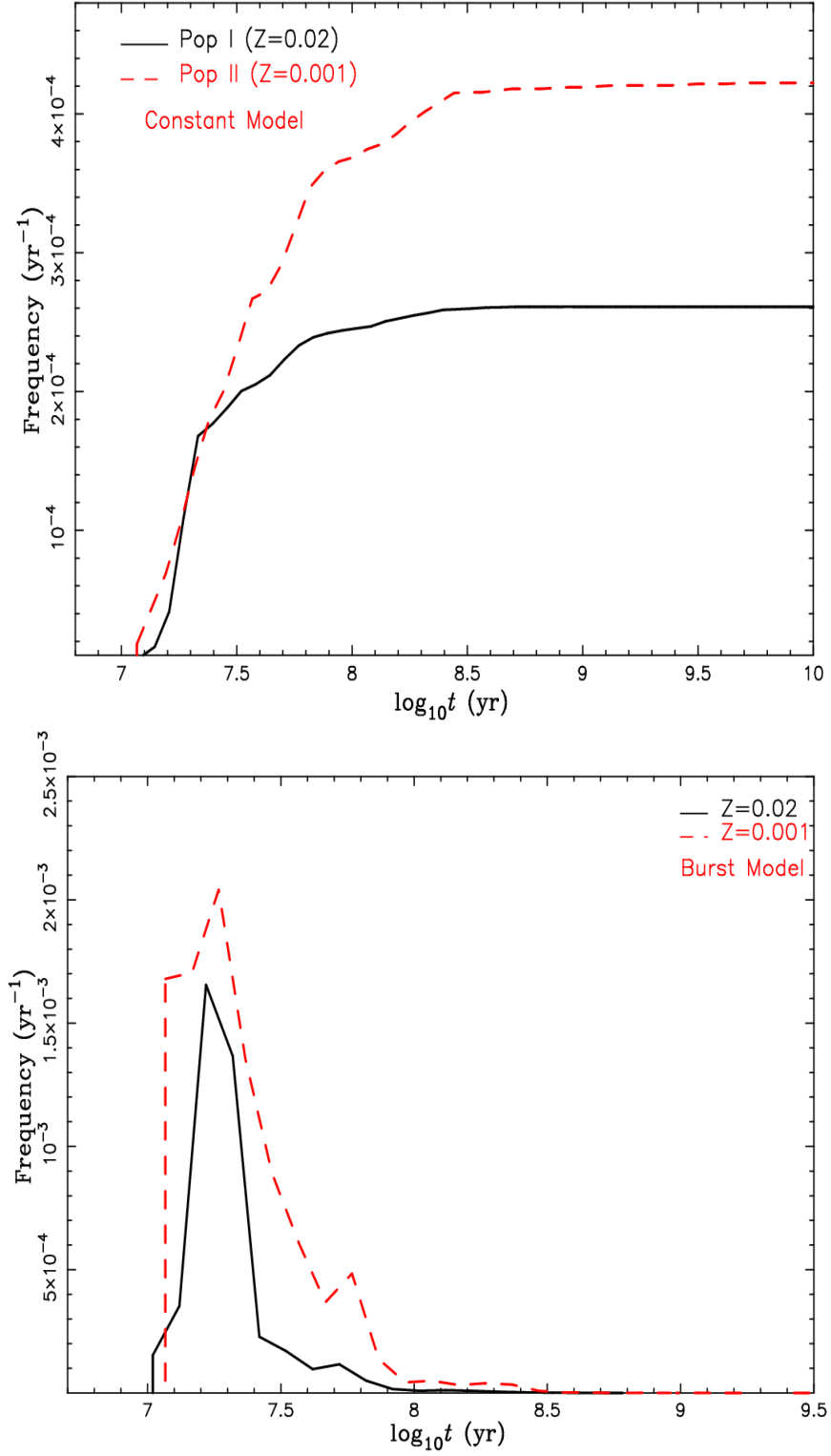


Fig. 5.— The rate evolutions of ULX pulsar binaries under a constant star formation model (upper) and single burst star formation model (lower).

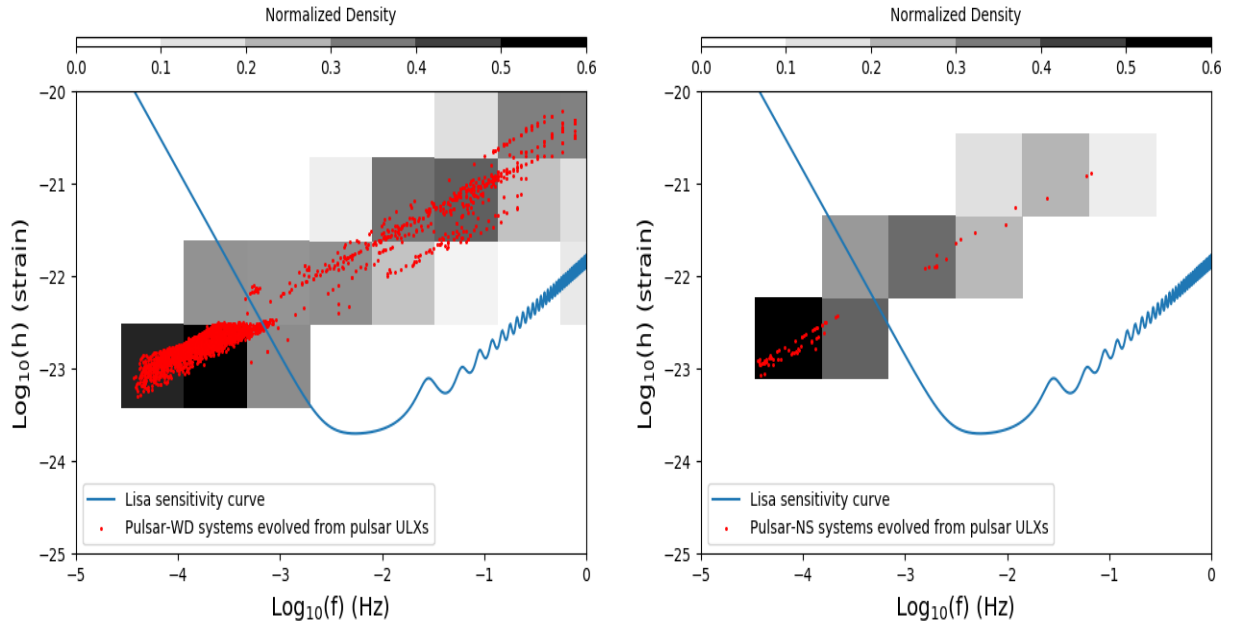


Fig. 6.— The distribution of GW-sources from NS-WD (right) and NS-NS (left panel) mergers in the strain-frequency space. The sources are assumed to be at 10 kpc distances. The sensitivity curve of LISA is shown with the solid blue line. Gray scale are all NS-WD and NS-NS sources in our simulation. Red dots are pulsar-WD and pulsar-NS sources evolved from ULX pulsar binaries.